EPJ Web of Conferences **274**, 02014 (2022) https://doi.org/10.1051/epjconf/202227402014
XVth Quark Confinement and the Hadron Spectrum

Roles of Polyakov loops in Yang-Mills theory on $\mathbb{T}^2 \times \mathbb{R}^2$

Daiki Suenaga[1,2,*] and *Masakiyo* Kitazawa[3,4,5,**]

[1]Strangeness Nuclear Physics Laboratory, RIKEN Nishina Center, Wako 351-0198, Japan
[2]Research Center for Nuclear Physics, Osaka University, Ibaraki 567-0048, Japan
[3]Yukawa Institute for Theoretical Physics, Kyoto University, Kyoto, 606-8502 Japan
[4]J-PARC Branch, KEK Theory Center, Institute of Particle and Nuclear Studies, KEK, 319-1106 Japan
[5]Department of Physics, Osaka University, Toyonaka, Osaka, 560-0043 Japan

Abstract. We present an effective model of SU(N) pure Yang-Mills theory on $\mathbb{T}^2 \times \mathbb{R}^2$, where two directions are compactified with periodic boundary conditions. Our model includes two Polyakov loops serving as the order parameters of two center symmetries. Based on the model, for $N = 2$ and $N = 3$ we show that a rich phase diagram in terms of the center symmetries on $\mathbb{T}^2 \times \mathbb{R}^2$ is obtained. Besides, we demonstrate roles of the Polyakov loops by comparing with the recent lattice results focusing on thermodynamic quantities on $\mathbb{T}^2 \times \mathbb{R}^2$. We expect that analysis on $\mathbb{T}^2 \times \mathbb{R}^2$ provides us with a new clue toward further understanding of pure YM theory with the Polyakov loop at finite temperature.

1 Introduction

Quantum effects triggered by a boundary condition (BC) exhibit characteristic phenomena that cannot be driven in the isotropic and infinitely large volume system. One striking example is the Casimir effect [1–3]; it was found that a force is certainly induced between two plates separated by a finite distance, even for a free theory. In this regard, finite-temperature effects are also understood as the BC one since such a system is realized by compactifying the imaginary time with period $1/T$ (T is the temperature).

The SU(N) Yang-Mills (YM) theory at finite T is known to provide us with new insights which cannot be gained in the vacuum. The emergence of center symmetry is one significant example. Center symmetry is related to the color confinement, i.e., the deconfined (confined) phase is realized when center symmetry is preserved (spontaneously broken). An order parameter of center symmetry, or the confinement-deconfinement phase transition, is the Polyakov loop (for the detail, see, e.g., Ref. [4] and references therein).

In this article, in order to pursue new aspects of the BC effects, we explore pure YM theory on a manifold $\mathbb{T}^2 \times \mathbb{R}^2$ where one spatial direction in addition to the imaginary time one is compactified [5]. In such a system, two center symmetries associated with two Polyakov loops emerge. Thus, we present an effective model for pure YM theory with the two Polyakov loops on $\mathbb{T}^2 \times \mathbb{R}^2$, and investigate a phase diagram focusing on center symmetries for $N = 2$ and $N = 3$.

Pure YM theory on $\mathbb{T}^2 \times \mathbb{R}^2$ can be surveyed by the *lattice simulation* [6, 7]. In particular, in Ref. [7], thermodynamic quantities such as the energy density and pressures on $\mathbb{T}^2 \times \mathbb{R}^2$ for

*e-mail: daiki.suenaga@riken.jp
**e-mail: kitazawa@yukawa.kyoto-u.ac.jp

SU(3) YM theory were investigated on the lattice, and it was found that a free massless theory cannot reproduce the lattice data even qualitatively, implying that nonperturbative effects of gauge theory are essential to explain them. Motivated by this fact, in the present article, we also investigate the thermodynamic quantities from our model to compare with the lattice data, and demonstrate roles of the two Polyakov loops on $\mathbb{T}^2 \times \mathbb{R}^2$.

This article is organized as follows. In Sec. 2, our effective model of SU(N) pure YM theory including two Polyakov loops on $\mathbb{T}^2 \times \mathbb{R}^2$ is introduced. Based on the model, in Sec. 3 we explore the phase diagram focusing on two center symmetries on $\mathbb{T}^2 \times \mathbb{R}^2$ for $N = 2$ and $N = 3$. Comparison between our model and the lattice data is made in Sec. 4, and we conclude the present work in Sec. 5.

2 Model

In this section, we introduce our model to explore the roles of two Polyakov loops on $\mathbb{T}^2 \times \mathbb{R}^2$. In the following analysis, we choose the imaginary time τ and one spatial coordinate x as the compactified directions: $\mathbb{T}^2 \cong \mathbb{S}^1 \times \mathbb{S}^1$, the lengths of which are L_τ and L_x, respectively. Meanwhile, the remaining y and z directions are left infinitely large and flat.

The Polyakov loops as the order parameters of two center symmetries $Z_N^{(\tau)} \times Z_N^{(x)}$ are introduced through background fields of the gauge field A_μ ($\mu = \tau, x, y, z$). In the present exploratory investigation, we assume that the background fields, which are $N \times N$ matrices in the color space, are homogeneous and diagonal for both τ and x components as

$$A_c = \frac{1}{L_c} \mathrm{diag}\Big[(\theta_c)_1, (\theta_c)_2, \cdots, (\theta_c)_N\Big] , \tag{1}$$

where $c = \tau, x$ stands for the compactified coordinates. The angles θ_c's satisfy the traceless condition of the SU(N) YM theory: $\sum_{i=1}^N (\theta_c)_i = 0$. From our ansatz (1), the Polyakov loops are evaluated to be

$$P_c = \frac{1}{N} \mathrm{Tr}\Big[\exp\left(iL_c A_c\right)\Big] = \frac{1}{N} \sum_{i=1}^{N} \mathrm{e}^{i(\theta_c)_i} . \tag{2}$$

As is well known, the temporal Polyakov loop P_τ not only serves as an order parameter of $Z_N^{(\tau)}$ center symmetry but also is related to the free energy F_q where one test particle is placed as $NP_\tau = \exp(-L_\tau F_q)$. That is, the physical role of P_τ is obvious; $P_\tau = 0$ ($P \neq 0$) represents the confinement phase (deconfinement phase). Meanwhile, the spatial Polyakov loop P_x does not show such a clear role. For this reason, we simply regard P_x as an order parameter of $Z_N^{(x)}$ center symmetry. In a limit of $L_\tau \to \infty$, we expect that the system is always governed by confined phase regardless of the value of L_x. That is, $P_\tau = 0$ is always satisfied at $L_\tau \to \infty$ for any L_x. By interchanging τ and x, one can also obtain $P_x = 0$ at $L_x \to \infty$ for any L_τ.

In Sec. 3, we present a phase diagram on the center symmetries for $N = 2$ and $N = 3$. In these gauge groups, we can parametrize the angles by a single parameter ϕ_c as

$$\begin{aligned} [(\theta_c)_1, (\theta_c)_2] &= (\phi_c, -\phi_c) \quad \text{for} \quad N = 2 , \\ [(\theta_c)_1, (\theta_c)_2, (\theta_c)_3] &= (\phi_c, 0, -\phi_c) \quad \text{for} \quad N = 3 , \end{aligned} \tag{3}$$

respectively. Accordingly, the Polyakov loop (2) is also expressed by ϕ_c solely as

$$\begin{aligned} P_c &= \cos\phi_c \quad \text{for} \quad N = 2 , \\ P_c &= \frac{1}{3}(1 + 2\cos\phi_c) \quad \text{for} \quad N = 3 . \end{aligned} \tag{4}$$

In our present study, we construct the free energy density f by referring to the model-B of Ref. [8], where the phase structures and thermodynamic properties of pure YM theory are investigated at finite temperature T, i.e., $\mathbb{S}^1 \times \mathbb{R}^3$. In this model, f is based on a sum of the perturbative term $f_{\rm pert}$ and the potential one $f_{\rm pot}$. The former describes one-loop contributions of the massless gauge field upon the background which leads to the deconfined phase at high T, while the latter is included to realize the confined phase at low T. In particular, the Haar measure potential motivated by the strong-coupling expansion is employed for $f_{\rm pot}$. The phase structure is determined as a result of competition between $f_{\rm pert}$ and $f_{\rm pot}$. As a naive extension of the model-B of Ref. [8] onto $\mathbb{T}^2 \times \mathbb{R}^2$, we take the following free energy density: $f = f_{\rm pert} + f_{\rm pot}$ with

$$f_{\rm pert} = \frac{2}{L_\tau L_x} \sum_{j,k=1}^{N} \left(1 - \frac{\delta_{jk}}{N}\right) \sum_{l_\tau, l_x} \int \frac{d^2 p_L}{(2\pi)^2} \ln\left[\left(\omega_\tau - \frac{(\Delta\theta_\tau)_{jk}}{L_\tau}\right)^2 + \left(\omega_x + \frac{(\Delta\theta_x)_{jk}}{L_x}\right)^2 + \boldsymbol{p}_L^2\right], \quad (5)$$

and

$$f_{\rm pot} = -\frac{1}{L_\tau R^3} \ln\Big[\prod_{j<k} \sin^2\left(\frac{(\Delta\theta_\tau)_{jk}}{2}\right)\Big] - \frac{1}{L_x R^3} \ln\Big[\prod_{j<k} \sin^2\left(\frac{(\Delta\theta_x)_{jk}}{2}\right)\Big]. \quad (6)$$

In these equations, we have defined $(\Delta\theta_c)_{jk} = (\theta_c)_j - (\theta_c)_k$ and $\boldsymbol{p}_L = (p_y, p_z)$. The "Matsubara frequencies" are given by $\omega_c = (2\pi l_c)/L_c$ to describe the periodic BC for both τ and x directions. Besides, the parameter R having mass dimension -1 determines the typical scale of phase transition points with respect to $Z_N^{(\tau)} \times Z_N^{(x)}$ center symmetries. It should be noted that, for $f_{\rm pot}$, separable ansatz where the interplay between temporal and spatial potentials is absent is used to demonstrate roles of two Polyakov loops clearly in the present exploratory work.

Before closing this section, for later convenience we present concrete forms of $f_{\rm pert}$ and $f_{\rm pot}$ for $N = 2$ and $N = 3$. Here, as for the perturbative term $f_{\rm pert}$, the momentum integral and Matsubara summation in Eq. (5) leads to ultraviolet (UV) divergences. To subtract the divergences, we make use of the dimensional regularization together with the inhomogeneous and generalized Epstein-Hurwitz zeta function [9]. The resulting regularized $f_{\rm pert}$ reads

$$\begin{aligned} f_{\rm pert} &= -\frac{\pi^2}{15L_\tau^4} + \frac{4\phi_\tau^2(\phi_\tau - \pi)^2}{3\pi^2 L_\tau^4} - \frac{\pi^2}{15L_x^4} + \frac{4\phi_x^2(\phi_x - \pi)^2}{3\pi^2 L_x^4} \\ &\quad -\frac{4}{\pi^2} \sum_{l_\tau, l_x=1}^{\infty} \frac{1 + 2\cos(2\phi_\tau l_\tau)\cos(2\phi_x l_x)}{X_{l_\tau, l_x}^4}, \end{aligned} \quad (7)$$

for $N = 2$, and

$$\begin{aligned} f_{\rm pert} &= -\frac{8\pi^2}{45L_\tau^4} + \frac{8\phi_\tau^2(\phi_\tau - \pi)^2 + \phi_\tau^2(\phi_\tau - 2\pi)^2}{6\pi^2 L_\tau^4} \\ &\quad -\frac{8\pi^2}{45L_x^4} + \frac{8\phi_x^2(\phi_x - \pi)^2 + \phi_x^2(\phi_x - 2\pi)^2}{6\pi^2 L_x^4} \\ &\quad -\frac{8}{\pi^2} \sum_{l_\tau, l_x=1}^{\infty} \frac{1}{X_{l_\tau, l_x}^4}\Big[1 + 2\cos(\phi_\tau l_\tau)\cos(\phi_x l_x) + \cos(2\phi_\tau l_\tau)\cos(2\phi_x l_x)\Big], \end{aligned} \quad (8)$$

for $N = 3$, with $X_{l_\tau, l_x} \equiv \sqrt{(l_\tau L_\tau)^2 + (l_x L_x)^2}$ [5]. The second line of Eq. (7) and the third line of Eq. (8) represent interplays between the BC effects from τ and x directions. Meanwhile,

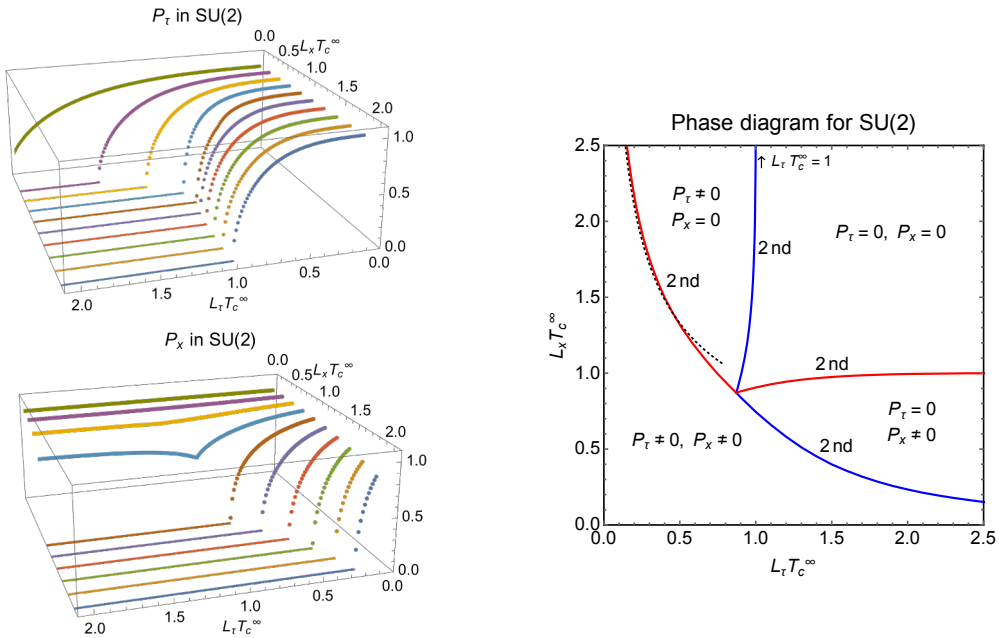

Figure 1. L_τ and L_x dependence of P_τ (upper-left panel) and P_x (lower-left panel) for $N = 2$. The right panel represents the corresponding phase diagram on L_τ - L_x plane. The detail is provided in the main text.

the potential term $f_{\rm pot}$ is straightforwardly evaluated from Eq. (6), yielding

$$f_{\rm pot} = -\frac{1}{L_\tau R^3}\ln(\sin^2\phi_\tau) - \frac{1}{L_x R^3}\ln(\sin^2\phi_x)\,, \tag{9}$$

for $N = 2$ and

$$f_{\rm pot} = -\frac{1}{L_\tau R^3}\ln\left[\left(\sin^4\frac{\phi_\tau}{2}\right)\left(\sin^2\phi_\tau\right)\right] - \frac{1}{L_x R^3}\ln\left[\left(\sin^4\frac{\phi_x}{2}\right)\left(\sin^2\phi_x\right)\right]\,, \tag{10}$$

for $N = 3$.

3 Phase diagram

In this section, based on the free energy density constructed in Sec. 2, we present the phase diagram focusing on two center symmetries $Z_N^{(\tau)} \times Z_N^{(x)}$ of pure YM theory on $\mathbb{T}^2 \times \mathbb{R}^2$ for $N = 2$ and $N = 3$. Extensions for $N \geq 4$ is straightforward.

3.1 $N = 2$

First, here we investigate the phase diagram for $N = 2$. As mentioned in Sec. 2, the Polyakov loops P_τ and P_x serve as the order parameters of $Z_2^{(\tau)}$ and $Z_2^{(x)}$ symmetries, respectively; the $Z_2^{(\tau)}$ ($Z_2^{(x)}$) symmetric phase is characteristic by $P_\tau = 0$ ($P_x = 0$), while the $Z_2^{(\tau)}$ ($Z_2^{(x)}$) symmetry-broken phase is by $P_\tau \neq 0$ ($P_x \neq 0$). In our model, the free energy density is not

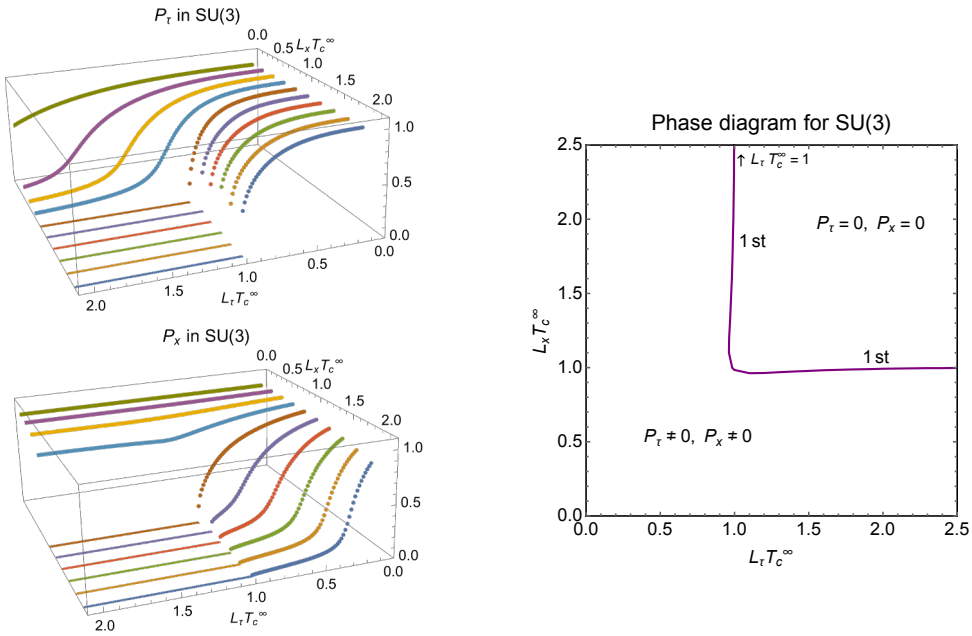

Figure 2. L_τ and L_x dependence of P_τ (upper-left panel) and P_x (lower-left panel) for $N = 3$. The right panel represents the corresponding phase diagram on L_τ - L_x plane. The detail is provided in the main text.

expressed in terms of the Polyakov loops P_τ and P_x directly but of the angles ϕ_τ and ϕ_x as seen in Eqs. (5) and (6). Hence, the phase diagram is drawn by seeking for a stationary point of $f = f_{\rm pert} + f_{\rm pot}$ with respect to ϕ_τ and ϕ_x.

Depicted in the upper-left and lower-left panels of Fig. 1 are the resultant L_τ and L_x dependence of the Polyakov loops P_τ and P_x, respectively. In the figure, the vertical and horizontal axes are normalized by multiplying T_c^∞ which represents the critical temperature for the confinement-deconfinement phase transition at $L_x \to \infty$. Within our model, T_c^∞ is evaluated to be $T_c^\infty = 1/[(2/3)^{1/3}R] \approx 1/(0.874R)$. For this reason, as seen from the upper-left panel, the phase transition of $Z_2^{(\tau)}$ symmetry breaking takes place at $L_x T_c^\infty = 1$. Besides, one can see that such a phase-transition point moves to smaller L_τ as L_x decreases from substantially large L_x, but for $L_x \lesssim 0.87$ the phase transition abruptly starts to occur at larger L_τ. Meanwhile, from the lower-left panel of Fig. 1, while P_x is always vanishing at $L_x \to \infty$, as L_x decreases one can find that the phase-transition point of $Z_N^{(x)}$ symmetry breaking appears. The point, however, disappears for $L_x T_c^\infty \lesssim 1$. All the phase transitions are found to be of second order.

In order to see the $Z_2^{(\tau)} \times Z_2^{(x)}$ symmetry properties on L_τ - L_x plane more clearly, we also display the corresponding phase diagram in the right panel of Fig. 1. The red (blue) curve represents the second-order phase-transition line distinguishing $P_x = 0$ and $P_x \neq 0$ ($P_\tau = 0$ and $P_\tau \neq 0$). The dotted curve is an analytic solution that indicates the phase-transition line evaluated by the Ginzburg-Landau analysis [5].

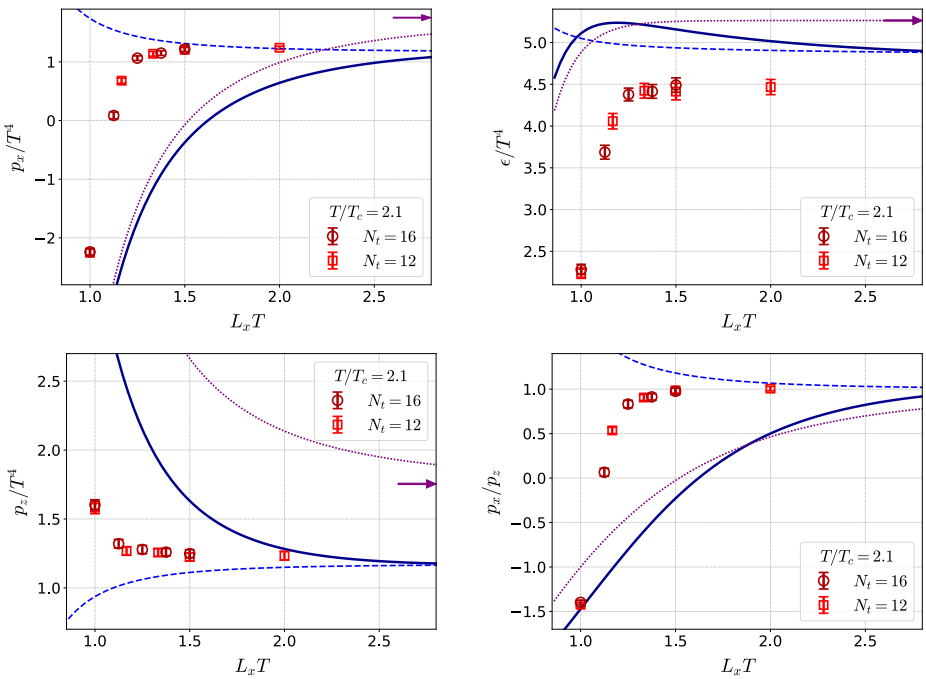

Figure 3. L_xT dependence of p_x (upper-left panel), p_z (lower-left panel) and ϵ (upper-right panel), normalized by T^4 with $T = 2.1T_c^\infty$. The lower-right panel represents the ratio p_x/p_z. The detail is provided in the main text.

3.2 $N = 3$

Next, we explore the phase diagram on $Z_3^{(\tau)} \times Z_3^{(x)}$ center symmetries for $N = 3$. Following a similar procedure to the analysis for $N = 2$, as displayed in Fig. 2, the resultant L_τ and L_x dependence of P_τ (upper-left panel) and P_x (lower-left panel), and the phase diagram (right panel) are obtained. The figure indicates that both the $Z_3^{(\tau)}$ and $Z_3^{(x)}$ symmetry breaking occurs at the identical line, and all the phase transitions are of first order. That is, the phase structures are obviously distinct from those for $N = 2$. Such differences are understood by the Ginzburg-Landau analysis as discussed in Ref. [5]. The phase diagram for $N \geq 4$ is expected to be similar to that for $N = 3$. We note that, e.g., the jump of P_x at the phase-transition point for $L_xT_c^\infty \gtrsim 1$ is comparably small, and eventually it vanishes at $L_x \to \infty$ to satisfy $P_x \to 0$ as argued in Sec. 2.

4 Thermodynamics

Gauge theory on a manifold $\mathbb{T}^2 \times \mathbb{R}^2$ can be surveyed by lattice simulations. In this regard, in Ref. [7], the L_x dependence of thermodynamic quantities such as the energy density and pressure of SU(3) pure YM theory above T_c^∞ was simulated on the lattice. In this section, we evaluate those physical quantities from our model to compare with the lattice results, and shed light on roles of the two Polyakov loops on $\mathbb{T}^2 \times \mathbb{R}^2$.

In our setting where the periodic BC is imposed along x direction, the stress tensor on the Minkowski space T^μ_ν can be diagonalized as $T^\mu_\nu = (\epsilon, p_x, p_y, p_z)$, with the energy density ϵ

and the pressure p_i ($i = x, y, z$). These values are derived by

$$\epsilon = \frac{L_\tau}{\mathcal{V}} \frac{\partial}{\partial L_\tau} \mathcal{V} f \quad , \quad p_i = -\frac{L_i}{\mathcal{V}} \frac{\partial}{\partial L_i} \mathcal{V} f \, , \tag{11}$$

where $\mathcal{V} = L_\tau L_x L_y L_z$ is the four-dimensional volume. We note that L_y and L_z are treated to be finite for a while, but after the derivatives we take $L_y, L_z \to \infty$. Since y and z directions are isotropic, in what follows, we only focus on ϵ, p_x and p_z.

Depicted in Fig. 3 is the resultant $L_x T$ ($= L_x/L_\tau$) dependence of the thermodynamic quantities for $T = 2.1T_c^\infty$ [$L_\tau = 1/T = 1/(2.1T_c^\infty)$]. The upper-left, lower-left, and upper-right panels represent p_x, p_z, and ϵ, respectively, normalized by T^4. In these panels, the solid curves are our model results for $N = 3$, whereas the dotted ones are the evaluation from a massless theory included as a reference. The arrow indicates the limiting value of the massless theory for $L_x \to \infty$. The lattice results [7] are denoted by the circle and square symbols for $N_\tau = 16$ and 12, respectively, where N_τ is the number of lattice sites along τ direction. This N_τ is related to the lattice spacing a by $N_\tau = (aT)^{-1}$. As seen from the panels, our model is not in good agreement with the lattice simulation data, particularly the persisting behavior of the data for $L_x T \gtrsim 1.5$, although the limiting value for $L_x \to \infty$ is improved from that of the massless theory.

From the panels, however, we can confirm that non-negligible contributions from the two Polyakov loops P_τ and P_x play an important role for thermodynamics on $\mathbb{T}^2 \times \mathbb{R}^2$. To see such importance, we also plot our model results where P_τ and P_x are fixed to be the limiting value at $L_x \to \infty$: $P_\tau \approx 0.973$ and $P_x = 0$, by the dashed curves in Fig. 3. The dashed curves do not change significantly down to $L_x T \simeq 1.5$ while our full results (solid curves) depart from the $L_x \to \infty$ value already at $L_x T \simeq 2.0$. In addition, the asymptotic directions of the dashed and solid curves for small L_x are opposite. Those variations clearly show that both the two Polyakov loops P_τ and P_x substantially affects the thermodynamics.

In order to cancel out the overall factors in different model evaluations, we depict the ratio p_x/p_z in the lower-right panel in Fig. 3. The panel also indicates similar behaviors as described above for the other panels.

Although we have failed in reproducing the lattice results on the thermodynamics from the present model satisfactorily, it has been confirmed that the two Polyakov loops P_τ and P_x play a significant role on $\mathbb{T}^2 \times \mathbb{R}^2$. It is expected that a more plausible model would be found by improving the potential term $f_{\rm pot}$.

5 Conclusions

In this article, we have presented an effective model of pure YM theory on $\mathbb{T}^2 \times \mathbb{R}^2$, by including two Polyakov loops along compactified directions. Based on the model, we have investigated the phase diagram on $\mathbb{T}^2 \times \mathbb{R}^2$ focusing on two center symmetries characterized by the Polyakov loops, and found a rich phase structures. We have also evaluated thermodynamic quantities such as the energy density and pressures to compare with the available lattice data [7]. From the analysis, it is found that two Polyakov loops play a significant role for the thermodynamics on $\mathbb{T}^2 \times \mathbb{R}^2$, although our model has failed in reproducing the lattice results satisfactorily.

The improved model which can reproduce the lattice results qualitatively would be obtained by modifying the potential of the Polyakov loops. Such an improved model is expected to provide us with a new clue toward further understanding of pure YM theory with the Polyakov loop at finite temperature. In addition to such a harvest, investigation of pure YM theory with the BC effects can be extended to other systems with, e.g., more compactifications, higher dimensions, and the anti-periodic BC in place of the periodic one. These

explorations would be reachable by the lattice simulations, and expected to lead to gaining new insights into the BC effects.

Acknowledgement

This work is supported by the RIKEN special postdoctoral researcher program (D. S.), and JSPS KAKENHI Grant Numbers JP19H05598, JP20H01903, JP22K03619 (M. K.).

References

[1] H.B.G. Casimir, Indag. Math. **10**, 261 (1948)
[2] S.K. Lamoreaux, Phys. Rev. Lett. **78**, 5 (1997), [Erratum: Phys.Rev.Lett. 81, 5475–5476 (1998)]
[3] U. Mohideen, A. Roy, Phys. Rev. Lett. **81**, 4549 (1998), `physics/9805038`
[4] K. Fukushima, V. Skokov, Prog. Part. Nucl. Phys. **96**, 154 (2017), `1705.00718`
[5] D. Suenaga, M. Kitazawa (2022), `2210.09363`
[6] M.N. Chernodub, V.A. Goy, A.V. Molochkov, Phys. Rev. D **99**, 074021 (2019), `1811.01550`
[7] M. Kitazawa, S. Mogliacci, I. Kolbé, W.A. Horowitz, Phys. Rev. D **99**, 094507 (2019), `1904.00241`
[8] P.N. Meisinger, T.R. Miller, M.C. Ogilvie, Phys. Rev. D **65**, 034009 (2002), `hep-ph/0108009`
[9] E. Elizalde, *Ten physical applications of spectral zeta functions*, Vol. 35 (1995), ISBN 978-3-642-29404-4, 978-3-642-29405-1